RESEARCH ARTICLE | MAY 05 2023

Dynamics of weak magnetic coupling by x-ray ferromagnetic resonance

Changsoo Kim; Won-Chang Choi; Kyoung-Woong Moon; ... et. al

Check for updates

CrossMark

View Online

Export Citation

Articles You May Be Interested In

Toward broad-band x-ray detected ferromagnetic resonance in longitudinal geometry

Journal of Applied Physics (June 2015)

Phase-resolved x-ray ferromagnetic resonance measurements in fluorescence yield

Journal of Applied Physics (April 2011)

Physics with gamma-beams and charged particle detectors: I) Nuclear structure II) Nuclear astrophysics

AIP Conference Proceedings (February 2015)

Dynamics of weak magnetic coupling by x-ray ferromagnetic resonance

View Online   Export Citation   CrossMark

Changsoo Kim,[1] Won-Chang Choi,[2] Kyoung-Woong Moon,[1] Hyun-Joong Kim,[1] Kyongmo An,[1] Byeong-Gyu Park,[3] Ho-young Kim,[4] Jung-il Hong,[2] Jaeyoung Kim,[5] Zi Q. Qiu,[6] Younghak Kim,[3,a] and Chanyong Hwang[1,a]

AFFILIATIONS

[1]Quantum Technology Institute, Korea Research Institute of Standards and Science, Daejeon 34113, Republic of Korea
[2]Department of Emerging Materials Science, Daegu Gyeongbuk Institute of Science and Technology, Daegu 42988, Republic of Korea
[3]Pohang Accelerator Laboratory, Pohang University of Science and Technology, Pohang 37673, Republic of Korea
[4]Max Plank POSTECH/Korea Center for Complex Phase Materials, Pohang 37673, Republic of Korea
[5]Center for Artificial Low Dimensional Electronic System, Institute for Basic Science, Pohang 37673, Republic of Korea
[6]Department of Physics, University of California at Berkeley, Berkeley, California 94720, USA

[a]Authors to whom correspondence should be addressed: iyhkim@postech.ac.kr and cyhwang@kriss.re.kr

ABSTRACT

We investigate the interaction between two magnetic layers separated with a normal metal insertion layer (Ti, Pt, and Ru) using x-ray ferromagnetic resonance (XFMR). We measure the amplitude and phase of the ferromagnetic resonance of both layers. Our results indicate that a ferromagnetic exchange coupling between two layers is a dominant coupling mechanism for a thick insertion metal layer. Based on the exchange coupling model, we extract the smallest value of the indirect exchange coefficient of $1.2\,\mu J/m^2$, which corresponds to an exchange field of about 0.36 mT. While this value is difficult to measure with other experimental tools, we were able to measure the small value because XFMR detects a resonance phenomenon of a thin layer generated by an oscillating indirect exchange and the Oersted fields with a phase and layer resolved observation.

I. INTRODUCTION

After the discovery of indirect exchange coupling, a ferromagnet (FM)/normal metal (NM)/ferromagnet or antiferromagnet (AFM)/NM/FM structure has been used to make magnetic field-free devices.[1–7] Since the indirect exchange coupling creates an effective magnetic field without any external magnetic field, they have great advantages for practical applications such as field-free magnetic-random access memory, stabilized skyrmion, guided spin wave, THz oscillator, and fast domain wall motion in synthetic antiferromagnets.[8–13] In spin valve systems, ferromagnetic resonance can transfer angular momentums from one magnetic layer to the other layer by spin pumping if the spin diffusion length is longer than normal metal thickness.[14–16]

When the interaction between two magnetic layers is relatively strong, or the thickness of the insertion layer is small, the interaction strength can be measured precisely with several conventional experimental tools.[2,3] However, the coupling between two distant magnetic layers has not been clearly quantified yet when the coupling strength is small. To detect such a small interaction strength, one suitable method is to utilize the resonance of magnetization. Under the magnetic resonance condition, the precession amplitude becomes large and exerts torques on adjacent layers. As a reciprocal process, resonant magnetization becomes affected by the external torques. This method has been used to investigate magnon–phonon and magnon–photon interactions.[17–22] In this article, we will show the detection of small interaction coupling strength in magnetic trilayer systems (FM/NM/FM) by using

x-ray ferromagnetic resonance (XFMR), which can provide information about the magnetization dynamics in layer-resolved or phase-resolved manners.[23–25]

The coupling between two distant magnetic layers can be established via either indirect exchange field or spin pumping mediated by electrons within a normal metal layer. It was also shown that an evanescent spin current could be transmitted through AFM.[26–33] Here, we show the interaction between two magnetizations with thick insertion layers using XFMR. We simulate two cases: two magnetic layers interacting with each other by (i) exchange interactions and (ii) spin pumping. We show that our

XFMR experiments can distinguish these two interactions. Our model agrees the experimental results well with parameters used in the simulations. The smallest interaction coefficient in our experiments was several times smaller than the value measured by other tools.

II. MODEL AND EXPERIMENT

First, we simulate the trilayer system using two coupled Landau–Lifshitz–Gilbert equations,

$$\frac{d\boldsymbol{m}_1}{dt} = -\gamma \left(\boldsymbol{m}_1 \times \boldsymbol{H}_{\text{eff, 1}} + \alpha_1 \left(\boldsymbol{m}_1 \times \frac{d\boldsymbol{m}_1}{dt} \right) - \alpha_{\text{sp,12}} \boldsymbol{m}_1 \times \left(\boldsymbol{m}_2 \times \frac{d\boldsymbol{m}_2}{dt} \right) \times \boldsymbol{m}_1 \right),$$

$$\frac{d\boldsymbol{m}_2}{dt} = -\gamma \left(\boldsymbol{m}_2 \times \boldsymbol{H}_{\text{eff,2}} + \alpha_2 \left(\boldsymbol{m}_2 \times \frac{d\boldsymbol{m}_2}{dt} \right) - \alpha_{\text{sp,21}} \boldsymbol{m}_2 \times \left(\boldsymbol{m}_1 \times \frac{d\boldsymbol{m}_1}{dt} \right) \times \boldsymbol{m}_2 \right),$$

$$\boldsymbol{H}_{\text{eff, i}} = \boldsymbol{H}_{\text{app}} + \boldsymbol{H}_{\text{d,i}} + \boldsymbol{H}_{\text{iex, i}} + \boldsymbol{H}_{\text{A, i}},$$

(1)

where $\boldsymbol{m}_i$ is a unit vector of the magnetization, γ is the gyromagnetic ratio, α_i is a damping constant, and $\alpha_{\text{sp,ij}}$ is a spin pumping coefficient, which represents the coupling by spin currents within the normal metal layer. $\boldsymbol{H}_{\text{eff,i}}$ includes an applied magnetic field ($\boldsymbol{H}_{\text{app}}$), demagnetization field ($\boldsymbol{H}_{\text{d,i}}$), an indirect exchange field from the other layer ($\boldsymbol{H}_{\text{iex, i}} = \frac{A_{\text{iex}}}{\mu_0 M_{\text{s,i}} \times t_{\text{FM,i}}} \boldsymbol{m}_j$), and an anisotropy field ($\boldsymbol{H}_{\text{A, i}} = \frac{K_{\text{A,i}}}{\mu_0 M_{\text{s,i}} \times t_{\text{FM,i}}} (\boldsymbol{m}_i \cdot \hat{\boldsymbol{z}})\hat{\boldsymbol{z}}$). A_{iex} is an indirect exchange constant, μ_0 is the vacuum magnetic permeability, $M_{\text{s,i}}$ is a saturated magnetization, $t_{\text{FM,i}}$ is a thickness of ferromagnet, and $K_{\text{A,i}}$ is the anisotropy constant. The parameters used in the simulation are shown in Table I. To simplify the model, we assumed that the total magnetic moment of the FM1 layer (50 nm) is 12 times larger than that of the FM2 layer (3 nm). In this case, FM2 is significantly affected by FM1 by the indirect exchange coupling and spin pumping, while FM1 is nearly not affected. We ignore the effect of indirect

exchange coupling and spin pumping at the FM1 layer in the simulation.

Figures 1(a) and 1(b) show the calculated magnetization dynamics of the two magnetic layers as a function of the magnetic field with different exchange coupling constants. Figure 1(c) shows the dynamics of only FM2 for various spin pumping coefficients. With decreasing coupling constant, FM2 becomes decoupled from FM1 and returns to an original resonance behavior, indicating that only the Oersted field from microwave current governs the dynamics of FM2. With increasing FM1's precessional amplitude, the torques by both the Oersted field and other coupling fields modulate the dynamics of FM2. In Figs. 1(a) and 1(b), the changes in lineshapes are opposite depending on the type of magnetic coupling order. This difference allows to distinguish ferromagnetic coupling and antiferromagnetic coupling. In Fig. 1(c), we find that the amplitude change by spin pumping is symmetric in contrast to the asymmetric changes by the indirect exchange couplings [see Figs. 1(a) and 1(b)]. In the cases of ferromagnetic and antiferromagnetic exchange fields, the large amount of phase shift is biased toward a field lower and higher from the FM1 peak, respectively, while a relatively small phase change occurs near the FM1 peak for the case of spin pumping. It should be noted that the sign of phase shift is inverted near the resonance peak of FM1 in Fig. 1(c). We used +90° to −90° phase notation rather than +180° to 0° for convenience.

We now show experimentally the observation of indirect coupling between two magnetic layers. To gain control over the interaction strength, we inserted NM layers (Ti, Pt, and Ru) or an insulating layer (MgO) between Py 50 nm and $Co_{40}Fe_{40}B_{20}$ 3 nm (CFB) on the silicon substrate covered with SiO_2. All samples were prepared with a structure of Py(50)/insertion layer/CFB(3)/Pt(2) by the RF and DC magnetron sputtering method. Since the total moment of the Py layer is 11.7–15.8 times larger than that of the

TABLE I. Simulation parameters for FM2 and CFB layers. For FM1 and Py, $M_{\text{s,1}} = 950$ kA/m, $K_{\text{A,1}} = 0$ mJ/m^2, and $\alpha_1 = 0.007$ were used except Fig. 7.

| Figure or sample	$M_{\text{s,2}}$ (kA/m)	$K_{\text{A,2}}$ (mJ/m^2)	α_2	A_{iex} (mJ/m^2)
Fig. 1	1300	0	0.04	in figures
Ti(2)	1200	0	0.07	0.0147
Ti(5)	1100	0	0.05	0.0041
Ti(10)	1100	0	0.05	0.0012
Ti(20)	1200	0	0.025	0
MgO(5)	1350	0	0.03	0
Pt(2)	1200	1.2	0.04	0.0224
Pt(5)	1200	1.2	0.06	0.0013
Ru(5)	1000	0	0.03	0.0034
Fig. 7	1300	0	in figures	0.001
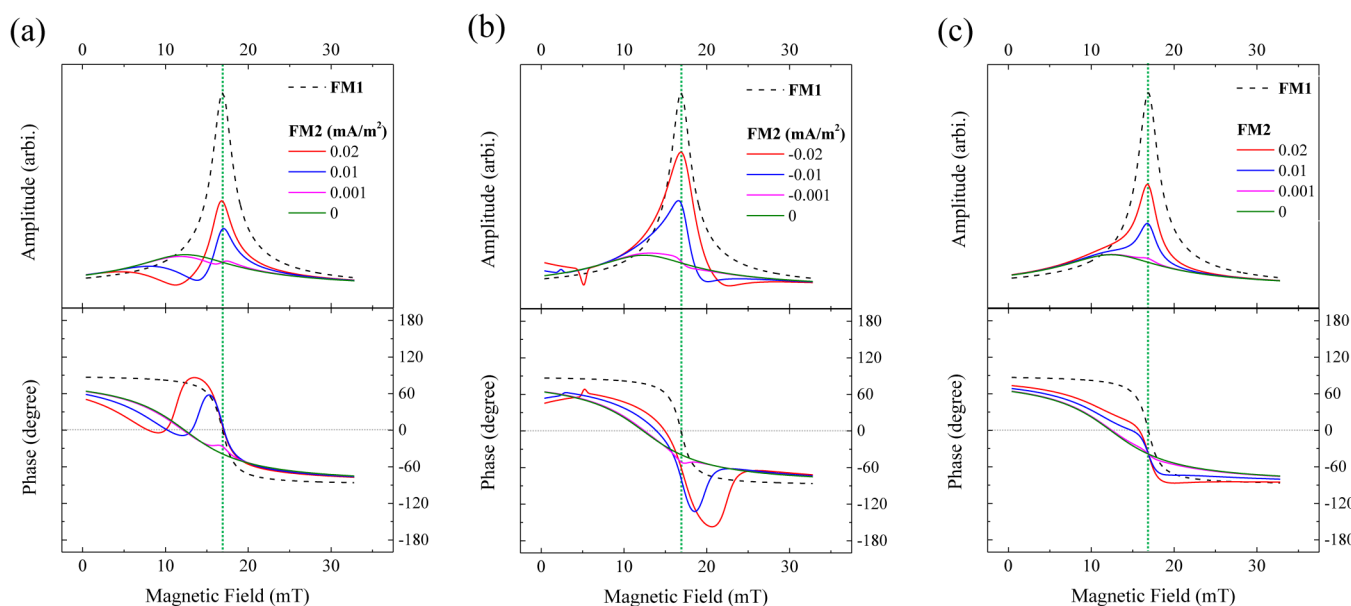
FIG. 1. Simulated dynamics of the weakly interacting magnetic layer (FM2) by (a) a ferromagnetic order, (b) an antiferromagnetic order, and (c) spin pumping depending on each coupling strength. FM1's dynamics are drawn by black dashed lines. Green dot lines are FM1's resonance peaks.

CFB layer, the precession of the Py layer is nearly unaffected by CFB, which is indeed close to the simulation condition.

Figure 2(a) shows the magnetic moments of prepared samples measured by vibrating sample magnetometry. In all data, the magnetic moments per unit area are nearly similar to each other, and small coercive fields (~0.4 mT) are observed. Normally, a double S-shape is found in the AFM order of indirect exchange interaction, which means a magnetic reversal by a spin-flop transition.[34] However, we cannot find a double S-shape in the hysteresis loops.

We observe the dynamics of two magnetic layers using XFMR at the 2A-MS beamline in PAL-II. XFMR technique can measure both the amplitude and phase of dynamic magnetization by utilizing x-ray magnetic circular dichroism. The x-ray beam is circularly polarized at a rate of over 80% between 100 and 1000 eV in the 2A-MS beamline. A 500 MHz radio frequency accelerating electrons along a storage ring is multiplied by 8 and amplified up to 26 dBm. We apply a 4 GHz microwave field to excite magnetizations by a shorted coplanar waveguide (CPWG). Through a 0.7 mm diameter hole, which is located
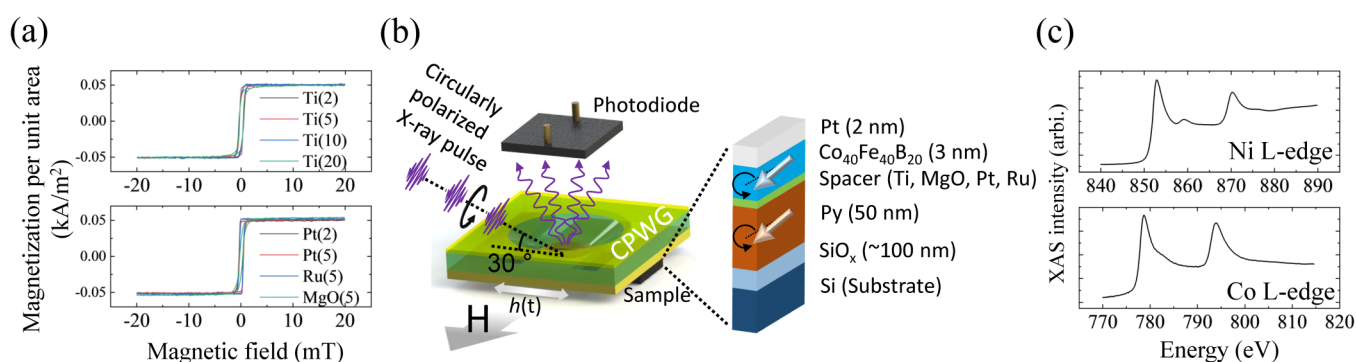

FIG. 2. (a) Magnetization data measured by vibrating sample magnetometry depending on the insertion layer. (b) Experimental configuration and sample structure. The sample is faced with the CPWG, which generates the oscillating Oersted field [h(t)] to excite the magnetizations (arrows in CFB and Py layers). The magnetic field (H) is applied to the sample's surface. The circularly polarized x-ray pulses are supplied with a grazing angle of 30° with respect to the sample surface. The CPWG has a tapered hole for a passway of x ray through the CPWG. (c) X-ray absorption spectra of CFB(3)/Ti(2)/Py(50) at Ni and Co L-edges.
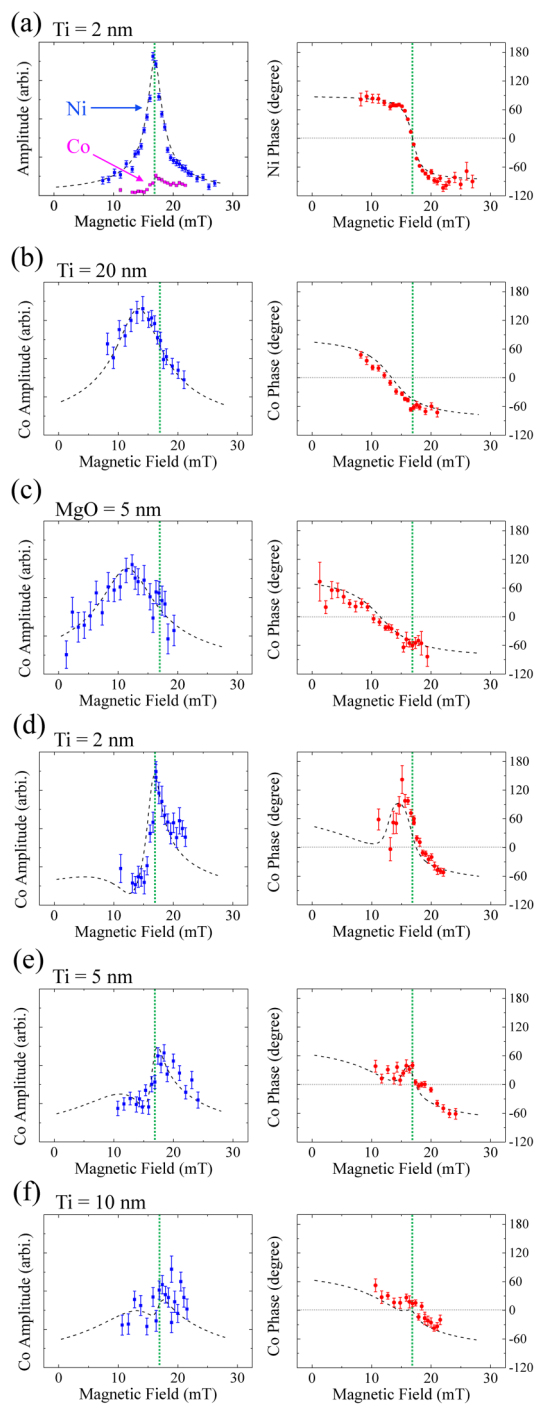
FIG. 3. Amplitude and phase obtained from the XFMR experiment using samples inserted with Ti or MgO layers. (a) Py's dynamics is shown when Ti(2) is inserted. In the amplitude section, Co's dynamics is shown for comparison. CFB's dynamics are drawn when (b) Ti(20), (c) MgO(5), (d) Ti(2), (e) Ti(5), and (f) Ti(10) are inserted. Green dot lines are Py's resonance peaks. Black dashed lines are simulated results.

1.2 mm away from the shorted end of the CPWG, a circularly polarized x ray is transferred to the sample surface facing the CPWG. Near the hole, the estimated Oersted field is about 60 μT. The x ray is incident with a 30° grazing angle. At peaks of Ni and Co L3 edges, we measure fluorescent signals from Py and CFB layers with an aluminum-coated silicon diode (AXUV100TF400, Opto Diode) and obtain sinusoidal curves at each magnetic field by a microwave phase delayer controlling the phase of 500 MHz radio frequency. All experiments are conducted at room temperature. A schematic diagram of the experimental setup is shown in Fig. 2(b).
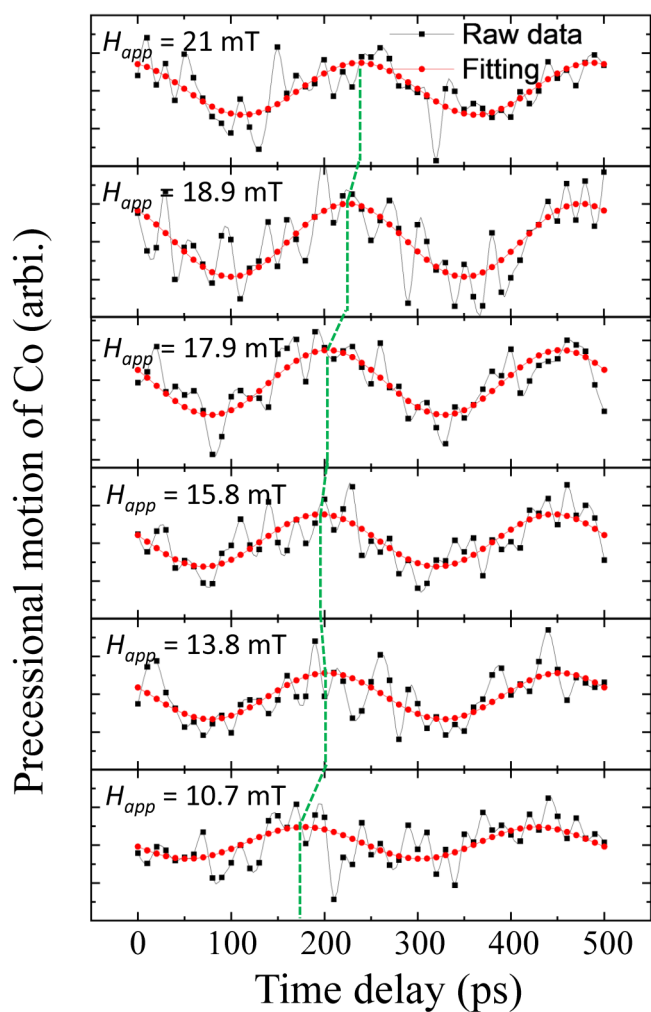

FIG. 4. Precession motion of the CFB layer with the Ti(2) insertion layer at each magnetic field depending on the time delay of microwave current. Black square and red circular mean the experimental data and fitting results, respectively. Green dashed lines indicate the amount of frequency shift among magnetic fields.

We measure the x-ray absorption of our samples in the XFMR configuration with the total fluorescent yield mode. Figure 2(c) shows the x-ray absorption spectra of the magnetic trilayer with the Ti(2) insertion layer at Ni and Co L-edges. The absorption lines of L3- and L2-edges are clearly visible, and the self-absorption effect appears in the L-edge. This is because the x-ray incident angle is inclined 30° from the sample's surface.[35,36]

III. ANALYSIS AND DISCUSSION

The amplitudes and phases of Py and CFB are extracted from the sinusoidal curves and depicted in Fig. 3. All samples exhibit a single Lorentzian and a 180° phase change at Ni's resonance in Fig. 3(a). Variation in the phase for Ni's resonance is shown in Fig. 3(a). All the Py spectra in our samples were similar, indicating that the dynamics of Py are hardly affected by CFB. In Fig. 3(b), with the Ti(20) insertion layer, the shape of the amplitude of CFB is symmetric and the phase monotonically decreases. The amplitude and phase are well fitted with a single Lorentzian, which is consistent with the negligible coupling across the thick Ti layer.
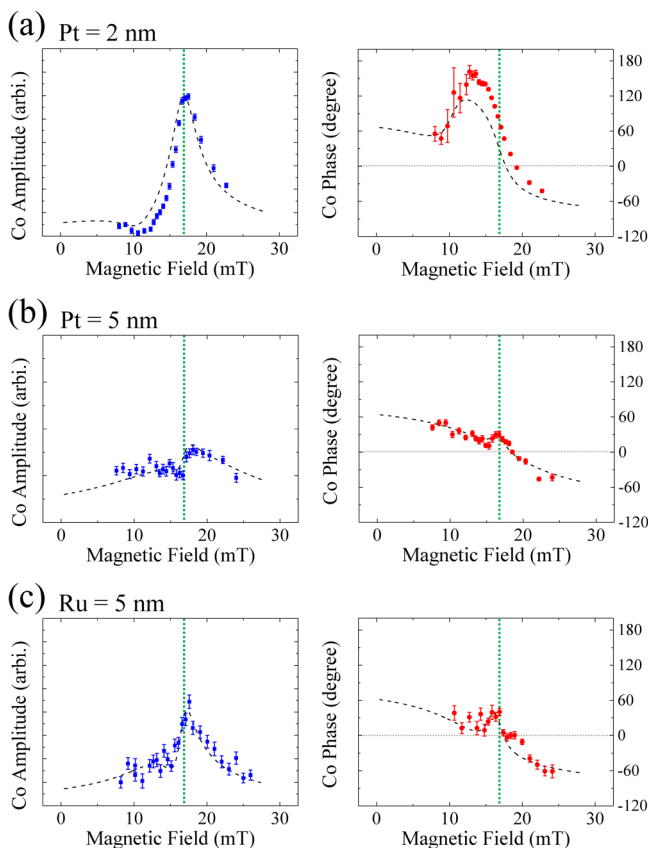

FIG. 5. CFB layer's amplitude and phase obtained from the XFMR experiment using samples inserted with (a) Pt(2), (b) Pt(5), and (c) Ru(5). Green dot lines are Py's resonance peaks. Black dashed lines are the simulated results.

This is proved by another XFMR result with MgO(5) depicted in Fig. 3(c), which shows a single ferromagnetic resonance. Considering that an insulating MgO(5) does not have itinerant electrons, two magnetic layers should not be coupled with the indirect exchange field and not be affected by spin pumping originating from Py's resonance.[37–39]

In contrast to the ordinary ferromagnetic resonance shown in the sample with Ti(20) or MgO(5) inserted, the dynamics in CFB are quite different from the single Lorentzian as shown in Figs. 3(d)–3(f). In Fig. 3(d), the amplitude peak is asymmetric and biased toward a high field where the Py resonance peak is located. The phase abruptly increases and decreases near Py's resonance peak. As the thickness of Ti increases, the amplitude of CFB near Py's resonance peak decreases and the phase change decreases. This abnormal CFB dynamics is attributed to the torque by the indirect exchange field from Py's resonance because the shapes of amplitude and phase are the most similar to the ferromagnetic indirect exchange coupling as shown in Fig. 1(a). The phase shift direction is not matched with that in the antiferromagnetic order [see Fig. 1(b)] and the phase is not inverted at the Py resonance, which is different from the spin pumping case [see Fig. 1(c)]. Considering the spin diffusion length of Ti of about 13.3 nm, the spin pumping effect is small due to the insertion layer.[40]

Comparing Figs. 3(b) and 3(d), the precessional motion is suppressed due to the competition between the oscillating Oersted field and the indirect exchange fields by Py at the CFB's resonance peak. Although the Oersted and indirect exchange field are perpendicular to each other at the peak of Py's resonance, the largest oscillating field is generated from the sum of these fields, which leads to the peak amplitude in CoFeB's precession. Above Py's resonance peak, the amplitudes are still enhanced because the Oersted field and the indirect exchange field tend to align parallel to each other. As the thickness of Ti increases, the influence of indirect exchange becomes weakened, which results in an independent magnetic resonance in
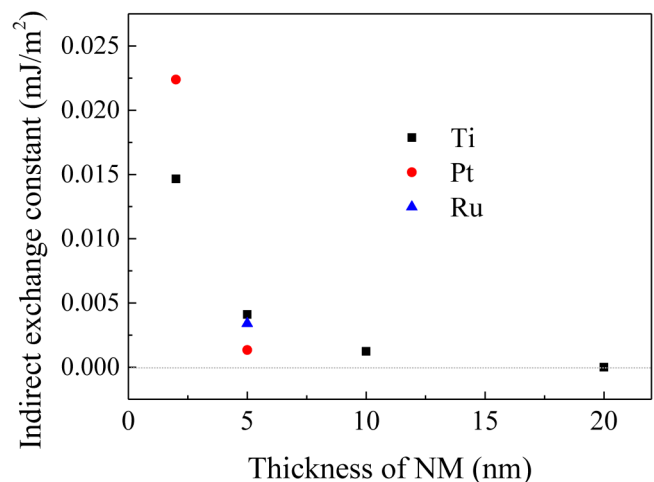
FIG. 6. Indirect exchange constants in the function of thickness of normal metal layers.

the sample with Ti(20) inserted. In Fig. 3(f), despite a bad signal-to-noise ratio, there is still interaction between Py and CFB because the signals near Py's resonance peak are still larger than those in the lower field area.

We show several precessional motions of Co magnetization in the trilayer with the Ti(10) insertion layer at different magnetic fields in Fig. 4. To obtain the amplitude and phase at each data of the magnetic field, we utilized the non-linear least square fitting method (Levenberg–Marquardt method) of the sinusoidal function with a fixed frequency of 4 GHz. Two periodic motions during 500 ps are clearly observed, and the phase change is stationary from 13.8 to 17.9 mT. In this region, the phase of Co is changed slightly from the original phase curve due to the weak indirect exchange interaction field generated by Py in a resonance state.

In Fig. 5, we show the XFMR experimental results with Pt and Ru insertion layers. We obtain the material parameters using the same process without spin pumping.[41,42] Based on the parameters of Figs. 3(a) and 3(b), we simulate the CFB dynamics and extract the material parameters at each insertion layer (Table I). The damping constant of CFB is rather larger than expected. All samples are capped with Pt(2), which is known as a good spin sinking layer.[43,44] Pumped spins into Ti, Pt, and MgO layers are attenuated and absorbed by the Py layer, which also increases the damping constants. In addition, there will be a lot of intermixing with the surrounding metallic layer from a large damping constant.[45–47] It is widely known that the growth mechanism of the magnetic thin film varies depending on the thickness and type of the underlayer.[48–51] For this reason, magnetization is different for each sample, and the total magnetic moment ratio between the Py layer and the CFB layer is 11.7 to 17 times. The

indirect exchange interaction constants by Ti, Pt, and Ru layers are depicted in Fig. 6. All simulated curves are shown in Figs. 3 and 5 with black dashed lines.

Indirect exchange coupling strength has been measured using the exchange bias field in AFM/NM/FM or antiferromagnetically coupled FM/NM/FM systems in M-H hysteresis.[3,4] However, it is hard to measure the exchange bias field below several mT due to an imperfection of calibration near zero magnetic field when ferromagnetic cores are used. Moreover, with ferromagnetically coupled FM/NM/FM without an anisotropy, the indirect exchange field cannot be measured because two magnetizations simultaneously rotate when the magnetic field crosses a zero field. The conventional ferromagnetic resonance method can detect ferromagnetic or antiferromagnetic orders between two ferromagnets by a shift of the resonance field. However, considering that this method needs the original resonance fields of each layer without interactions, slightly different magnetizations between samples can lead to significant errors, particularly at a weak interaction.

We were able to measure the small exchange field because we used the resonance phenomena of the CFB layer. XMFR is free from the problems of static field measurement because it observes the dynamics generated from the two competing and oscillating fields in the same sample. In addition, since the Oersted field is as small as 0.1 mT, a small indirect exchange field can be measured by XFMR. In Fig. 6, the indirect exchange interaction constant of Ti(10) and Pt(5) is 1.2 μJ/m², which is 9 times smaller than the reported coupling constant of 10 μJ/m² measured by XFMR.[26]

Motivated by the detection of a small indirect exchange field in our experiments, we further investigate the role of difference in magnetization between two adjacent layers in the exchange-coupled
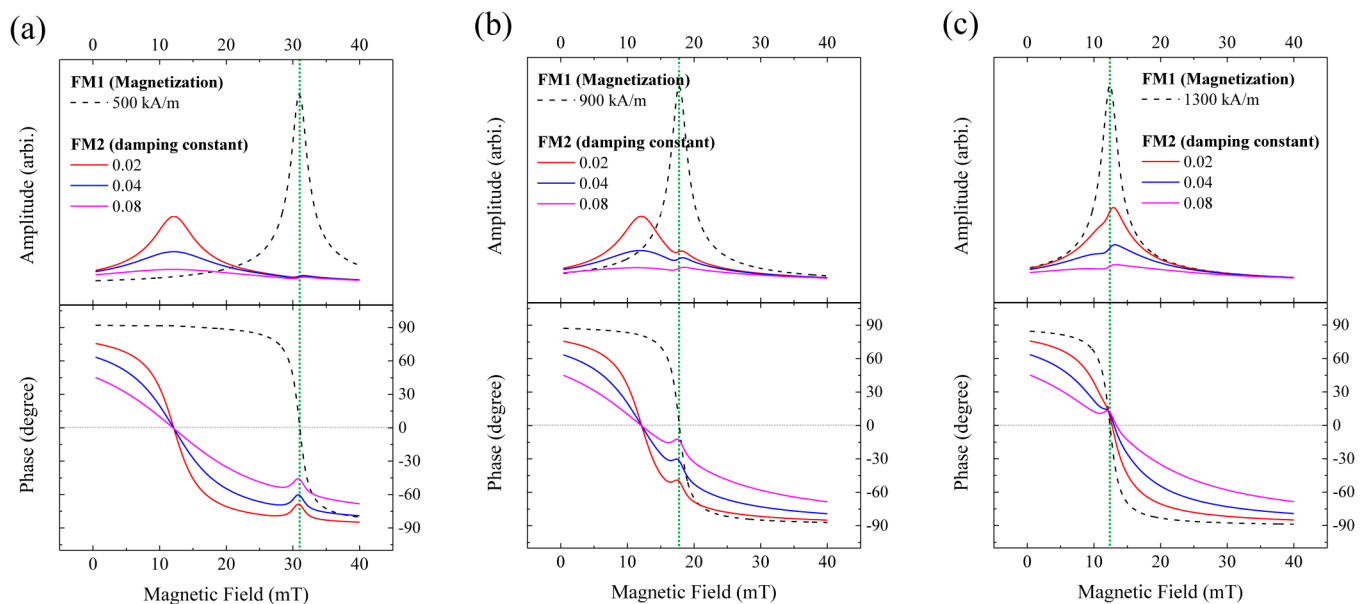
FIG. 7. Simulated dynamics of the weakly interacting magnetic layer (FM2) depending on the damping constant of FM2 and magnetization of FM1. Magnetizations of (a) 500, (b) 900, and (c) 1300 kA/m were used on the graphs. FM1's dynamics are drawn by black dashed lines. Green dot lines are FM1's resonance peaks.

system. In Fig. 7(a), FM1's resonance peak is far from FM2's due to a small magnetization. Although the damping constants of FM2 are different, the precessional amplitude and phase change by the indirect exchange interaction ($A_\mathrm{iex} = 1\,\mu\mathrm{J/m}^2$) almost remain constant. When the resonance peak of FM1 is close to that of FM2, the amount of phase change is not affected because the magnitude and direction of the total oscillating field generated by the Oersted field and FM1's resonance are the same in different magnetizations of FM1 [Fig. 7(b)]. On the other hand, the precession amplitude of FM2 is significantly amplified by 1.5, 2.3, and 2.9 times with damping constants of 0.08, 0.04, and 0.02 since the magnetization of FM2 does resonate by the total oscillating field. This means that we can obtain the same amount of phase change with better signal-to-noise ratios when we use the resonance phenomena of FM2. As the XFMR experiment takes several hours to obtain one spectrum, it would be essential to use this improvement for detecting the weak interaction. If the resonance lines of FM1 and FM2 overlap, the precessional amplitude increases, but the phase change is not significantly seen due to the rapid change of the background phase [Fig. 7(c)]. It would be necessary to adjust resonance fields and damping constants according to an experimental purpose.

IV. CONCLUSIONS

We conducted XFMR experiments to investigate the types of interactions between two magnetic layers in thin ferromagnet/normal metal/thick ferromagnet structures. Among the ferromagnetic, antiferromagnetic orders, and the spin pumping models, our experimental results are well agreed with the weakly interacting ferromagnetic model. The interaction strength monotonically decreases with the normal metal layer thickness. The lowest value of the experimentally detected indirect exchange interaction strengths was about $1.2\,\mu\mathrm{J/m}^2$, which corresponds to an exchange field of 0.36 mT. Our study proposes the use of XFMR to estimate the coupling strength especially in the weak coupling cases via the dynamics of coupled magnets.

ACKNOWLEDGMENTS

AUTHOR DECLARATIONS

Conflict of Interest

The authors have no conflicts to disclose.

Author Contributions

Changsoo Kim: Conceptualization (lead); Formal analysis (equal); Investigation (lead); Methodology (lead); Visualization (equal); Writing – original draft (equal); Writing – review & editing (equal). **Won-Chang Choi:** Data curation (equal); Methodology (equal). **Kyoung-Woong Moon:** Data curation (equal); Software (equal); Visualization (equal). **Hyun-Joong Kim:** Software (equal). **Kyongmo An:** Data curation (equal); Methodology (equal). **Byeong-Gyu Park:** Methodology (equal). **Ho-young Kim:** Methodology (equal). **Jung-il Hong:** Methodology (equal); Supervision (equal). **Jaeyoung Kim:** Methodology (equal); Supervision (equal). **Zi Q. Qiu:** Methodology (equal); Supervision (equal). **Younghak Kim:** Methodology (equal); Supervision (equal). **Chanyong Hwang:** Conceptualization (equal); Funding acquisition (equal); Project administration (equal); Supervision (equal); Writing – original draft (equal); Writing – review & editing (equal).

DATA AVAILABILITY

The data that support the findings of this study are available from the corresponding authors upon reasonable request.

REFERENCES

[1] S. S. P. Parkin, N. More, and K. P. Roche, Phys. Rev. Lett. **64**, 2304 (1990).

[2] S. S. P. Parkin, R. Bhadra, and K. P. Roche, Phys. Rev. Lett. **66**, 2152 (1991).

[3] S. S. P. Parkin, Phys. Rev. Lett. **67**, 3598 (1991).

[4] N. J. Gökemeijer, T. Ambrose, and C. L. Chien, Phys. Rev. Lett. **79**, 4270 (1997).

[5] J. Nogués and I. K. Schuller, J. Magn. Magn. Mater. **192**, 203 (1999).

[6] M. D. Stiles, J. Magn. Magn. Mater. **200**, 322 (1999).

[7] P. Bruno, J. Phys.: Condens. Matter **11**, 9403 (1999).

[8] D. C. Worledge, G. Hu, D. W. Abraham, J. Z. Sun, P. L. Trouilloud, J. Nowak, S. Brown, M. C. Gaidis, E. J. O´Sullivan, and R. P. Robertazzi, Appl. Phys. Lett. **98**, 022501 (2011).

[9] W. Legrand, D. Maccariello, F. Ajejas, S. Collin, A. Vecchiola, K. Bouzehouane, N. Reyren, V. Cros, and A. Fert, Nat. Mater. **19**, 34 (2020).

[10] E. Albisetti, D. Petti, M. Pancaldi, M. Madami, S. Tacchi, J. Curtis, W. P. King, A. Papp, G. Csaba, W. Porod, P. Vavassori, E. Riedo, and R. Bertacco, Nat. Nanotechnol. **11**, 545 (2016).

[11] B. Jiang, W. Zhang, H. Zhong, Y. Zhang, S. Yu, G. Han, S. Xiao, G. Liu, S. Yan, J. Li, and S. Kang, J. Magn. Magn. Mater. **490**, 165470 (2019).

[12] H. Zhong, S. Qiao, S. Yan, L. Liang, Y. Zhao, and S. Kang, J. Magn. Magn. Mater. **497**, 166070 (2020).

[13] S. H. Yang, K. S. Ryu, and S. Parkin, Nat. Nanotechnol. **10**, 221 (2015).

[14] Y. Tserkovnyak, A. Brataas, and G. E. W. Bauer, Phys. Rev. B **66**, 224403 (2002).

[15] B. Heinrich, Y. Tserkovnyak, G. Woltersdorf, A. Brataas, R. Urban, and G. E. W. Bauer, Phys. Rev. Lett. **90**, 187601 (2003).

[16] Y. Tserkovnyak, A. Brataas, G. E. W. Bauer, and B. I. Halperin, Rev. Mod. Phys. **77**, 1375 (2005).

[17] K. An, R. Kohno, A. N. Litvinenko, R. L. Seeger, V. V. Naletov, L. Vila, G. de Loubens, J. Ben Youssef, N. Vukadinovic, G. E. W. Bauer, A. N. Slavin, V. S. Tiberkevich, and O. Klein, Phys. Rev. X **12**, 011060 (2022).

[18] R. Schlitz, L. Siegl, T. Sato, W. Yu, G. E. W. Bauer, H. Huebl, and S. T. B. Goennenwein, Phys. Rev. B **106**, 14407 (2022).

[19] X. Zhang, C.-L. Zou, L. Jiang, and H. X. Tang, Phys. Rev. Lett. **113**, 156401 (2014).

[20] B. Bhoi, B. Kim, J. Kim, Y.-J. Cho, and S.-K. Kim, Sci. Rep. **7**, 11930 (2017).

[21] C. Berk, M. Jaris, W. Yang, S. Dhuey, S. Cabrini, and H. Schmidt, Nat. Commun. **10**, 2652 (2019).

[22] I. A. Golovchanskiy, N. N. Abramov, V. S. Stolyarov, M. Weides, V. V. Ryazanov, A. A. Golubov, A. V. Ustinov, and M. Y. Kupriyanov, Sci. Adv. **7**, eabe8638 (2021).

[23] C. Klewe, Q. Li, M. Yang, A. T. N´Diaye, D. M. Burn, T. Hesjedal, A. I. Figueroa, C. Hwang, J. Li, R. J. Hicken, P. Shafer, E. Arenholz, G. van der Laan, and Z. Qiu, Synchrotron Radiat. News **33**, 12 (2020).

[24] G. van der Laan, J. Electron Spectrosc. Relat. Phenome. **220**, 137 (2017).

[25] G. Boero, S. Mouaziz, S. Rusponi, P. Bencok, F. Nolting, S. Stepanow, and P. Gambardella, New J. Phys. **10**, 013011 (2008).

[26]D. A. Arena, E. Vescovo, C.-C. Kao, Y. Guan, and W. E. Bailey, Phys. Rev. B **74**, 064409 (2006).

[27]L. Gladczuk, L. Gladczuk, P. Dluzewski, K. Lasek, P. Aleshkevych, D. M. Burn, G. van der Laan, and T. Hesjedal, Phys. Rev. B **103**, 064416 (2021).

[28]A. A. Baker, A. I. Figueroa, C. J. Love, S. A. Cavill, T. Hesjedal, and G. van der Laan, Phys. Rev. Lett. **116**, 047201 (2016).

[29]J. Li, L. R. Shelford, P. Shafer, A. Tan, J. X. Deng, P. S. Keatley, C. Hwang, E. Arenholz, G. van der Laan, R. J. Hicken, and Z. Q. Qiu, Phys. Rev. Lett. **117**, 076602 (2016).

[30]C. J. Durrant, L. R. Shelford, R. A. J. Valkass, R. J. Hicken, A. I. Figueroa, A. A. Baker, G. van der Laan, L. B. Duffy, P. Shafer, C. Klewe, E. Arenholz, S. A. Cavill, J. R. Childress, and J. A. Katine, Phys. Rev. B **96**, 144421 (2017).

[31]Q. Li, M. Yang, C. Klewe, P. Shafer, A. T. N'Diaye, D. Hou, T. Y. Wang, N. Gao, E. Saitoh, C. Hwang, R. J. Hicken, J. Li, E. Arenholz, and Z. Q. Qiu, Nat. Commun. **10**, 5265 (2019).

[32]Y. Pogoryelov, M. Pereiro, S. Jana, A. Kumar, S. Akansel, M. Ranjbar, D. Thonig, D. Primetzhofer, P. Svedlindh, J. Åkerman, O. Eriksson, O. Karis, and D. A. Arena, Phys. Rev. B **101**, 054401 (2020).

[33]M. Dąbrowski, T. Nakano, D. M. Burn, A. Frisk, D. G. Newman, C. Klewe, Q. Li, M. Yang, P. Shafer, E. Arenholz, T. Hesjedal, G. van der Laan, Z. Q. Qiu, and R. J. Hicken, Phys. Rev. Lett. **124**, 217201 (2020).

[34]Q. Yang, L. Wang, Z. Zhou, L. Wang, Y. Zhang, S. Zhao, G. Dong, Y. Cheng, T. Min, Z. Hu, W. Chen, K. Xia, and M. Liu, Nat. Commun. **9**, 991 (2018).

[35]L. Tröger, D. Arvanitis, K. Baberschke, H. Michaelis, U. Grimm, and E. Zschech, Phys. Rev. B **46**, 3283 (1992).

[36]E. Zschech, L. Tröger, D. Arvanitis, H. Michaelis, U. Grimm, and K. Baberschke, Solid State Commun. **82**, 1 (1992).

[37]A. A. Baker, A. I. Figueroa, D. Pingstone, V. K. Lazarov, G. van der Laan, and T. Hesjedal, Sci. Rep. **6**, 35582 (2016).

[38]L. Mihalceanu, S. Keller, J. Greser, D. Karfaridis, K. Simeonidis, G. Vourlias, T. Kehagias, A. Conca, B. Hillebrands, and E. T. Papaioannou, Appl. Phys. Lett. **110**, 252406 (2017).

[39]C. Swindells, A. T. Hindmarch, A. J. Gallant, and D. Atkinson, Appl. Phys. Lett. **116**, 042403 (2020).

[40]C. Du, H. Wang, P. C. Hammel, and F. Yang, J. Appl. Phys. **117**, 172603 (2015).

[41]K. Roy, Phys. Rev. B **96**, 174432 (2017).

[42]S. Yakata, Y. Ando, T. Miyazaki, and S. Mizukami, Jpn. J. Appl. Phys., Part 1 **45**, 3892 (2006).

[43]M. Belmeguenai, M. S. Gabor, F. Zighem, N. Challab, T. Petrisor, R. B. Mos, and C. Tiusan, J. Phys. D: Appl. Phys. **51**, 045002 (2018).

[44]W. Cao, L. Yang, S. Auffret, and W. E. Bailey, Phys. Rev. B **99**, 094406 (2019).

[45]J. A. King, A. Ganguly, D. M. Burn, S. Pal, E. A. Sallabank, T. P. A. Hase, A. T. Hindmarch, A. Barman, and D. Atkinson, Appl. Phys. Lett. **104**, 242410 (2014).

[46]A. Ganguly, S. Azzawi, S. Saha, J. A. King, R. M. Rowan-Robinson, A. T. Hindmarch, J. Sinha, D. Atkinson, and A. Barman, Sci. Rep. **5**, 17596 (2015).

[47]S. Azzawi, A. Ganguly, M. Tokaç, R. M. Rowan-Robinson, J. Sinha, A. T. Hindmarch, A. Barman, and D. Atkinson, Phys. Rev. B **93**, 054402 (2016).

[48]R. D. McMichael, C. G. Lee, J. E. Bonevich, P. J. Chen, W. Miller, and W. F. Egelhoff, J. Appl. Phys. **88**, 5296 (2000).

[49]Z. Lu, Y. Fukuma, W. H. Butler, H. Fujiwara, G. J. Mankey, and S. Matsunuma, IEEE Trans. Magn. **45**, 4008 (2009).

[50]L. Cabral, F. H. Aragón, L. Villegas-Lelovsky, M. P. Lima, W. A. A. Macedo, and J. L. F. Da Silva, ACS Appl. Mater. Interfaces **11**, 1529 (2019).

[51]A. Acosta, K. Fitzell, J. D. Schneider, C. Dong, Z. Yao, R. Sheil, Y. E. Wang, G. P. Carman, N. X. Sun, and J. P. Chang, J. Appl. Phys. **128**, 013903 (2020).